Maximizing the value of 3D seismic data for shallow geohazard identification

James Selvage,[1*] Charles Jones[1] and Jonathan Edgar[2] describe methods to detect and analyze geohazards using 3D seismic data. They discuss the suitability of 3D seismic data for this purpose and the future directions for automating and improving seismic geohazard detection.

It has been recognized that 3D seismic data is often suitable as the basis for shallow geohazard analysis (OGP, 2011). In this article we present our experience of reprocessing and interpreting existing 3D seismic data for this purpose. The OGP Report No. 373-18-1 'Guidelines for the conduct of offshore drilling hazard site surveys' released during April 2011 provides guidelines on 'the use of exploration 3D seismic data to enhance, or to replace, acquisition of a site survey'. We hope that this article complements these guidelines and provides practical examples of how 3D seismic data can be processed and interpreted for geohazard identification and subsequent analysis.

To ensure confident detection of geohazards it is necessary to perform a comprehensive analysis of available data. Delivering this analysis in accordance with the drilling schedule is essential for operational safety.

We begin by discussing and attempting to demonstrate why bandwidth preservation is important when producing high fidelity seismic data for geohazard detection. Preserving bandwidth should be a primary objective of our processing (and acquisition). A processing sequence designed to maximize bandwidth in the shallow section from 3D seismic data is discussed. Then a comparison of 2D site survey seismic data versus reprocessed 3D seismic data is made in the context of geohazard analysis. A clear benefit of 3D seismic data is the ability to move beyond 2D interpretation into a 3D global interpretation approach. Global interpretation methods attempt to track every event in the 3D seismic data (Lomask and Guitton, 2007). These methods may be employed for shallow geohazard analysis and we demonstrate the use of a global interpretation algorithm for this purpose. A further benefit of 3D seismic data is the increased spatial accuracy and reliability of post- and pre-stack amplitudes. This enables volume-based and amplitude-versus-angle (AVA) based attributes to be generated and interpreted. Analysis can also be performed on stratigraphically consistent slices generated from the global interpretation approach. In summary our methodology for exploiting 3D seismic data entails:

- Reprocessing (or parallel processing) to achieve broader (frequency) bandwidth 3D seismic data,
- Performing pseudo-stratigraphic interpretation of the shallow section using a global interpretation algorithm,
- Using amplitude variation with angle/offset (AVA/O) information to analyze geohazards.

Our intention is to enable geohazard specialists to spend the majority of their time analyzing the risks caused by potential geohazards, as opposed to searching for them.

The importance of bandwidth

As stated by Sheriff (1991) resolution is the ability to separate two features that are very close together or, equivalently, the minimum separation of two bodies before their individual identities are lost. Seismic data involves both vertical and horizontal resolution. These are not independent; improving one automatically improves the other (Lindsey, 1989). Typically we consider that the resolving power of seismic is governed by frequency content, geological variability (velocity variability) and noise level.

In Figure 1 the importance of maintaining seismic bandwidth is illustrated. We begin with a broad bandwidth reflectivity series, which is generated from a broad bandwidth impedance series. Note that all frequencies are required to represent an impulse response, but we see notches in the amplitude spectrum that relate to the periodicity between impulses. To illustrate the impact of a reduction in bandwidth the reflectivity series is bandpass filtered to represent the bandwidth typical of 3D seismic surveys and 2D site surveys (the latter of which are often described as 'high-resolution'). In both cases when low frequencies are removed we observe that the broad bandwidth impedance log becomes relative and erroneous ramps are introduced. If the bandwidth is further reduced by removing high frequencies the character of both the reflectivity and impedance is further altered and this introduces further ambiguity into the interpretation. In particular it is less obvious where low amplitude reflection events occur due to the amplification of sidelobes.

[1] *Geophysical Operations, BG Group, Group, Reading, UK.*
[2] *Advanced Geoscience Team, BG Group, Group, Reading, UK.*
[*] *Corresponding author, E-mail: james.selvage@bg-group.com*

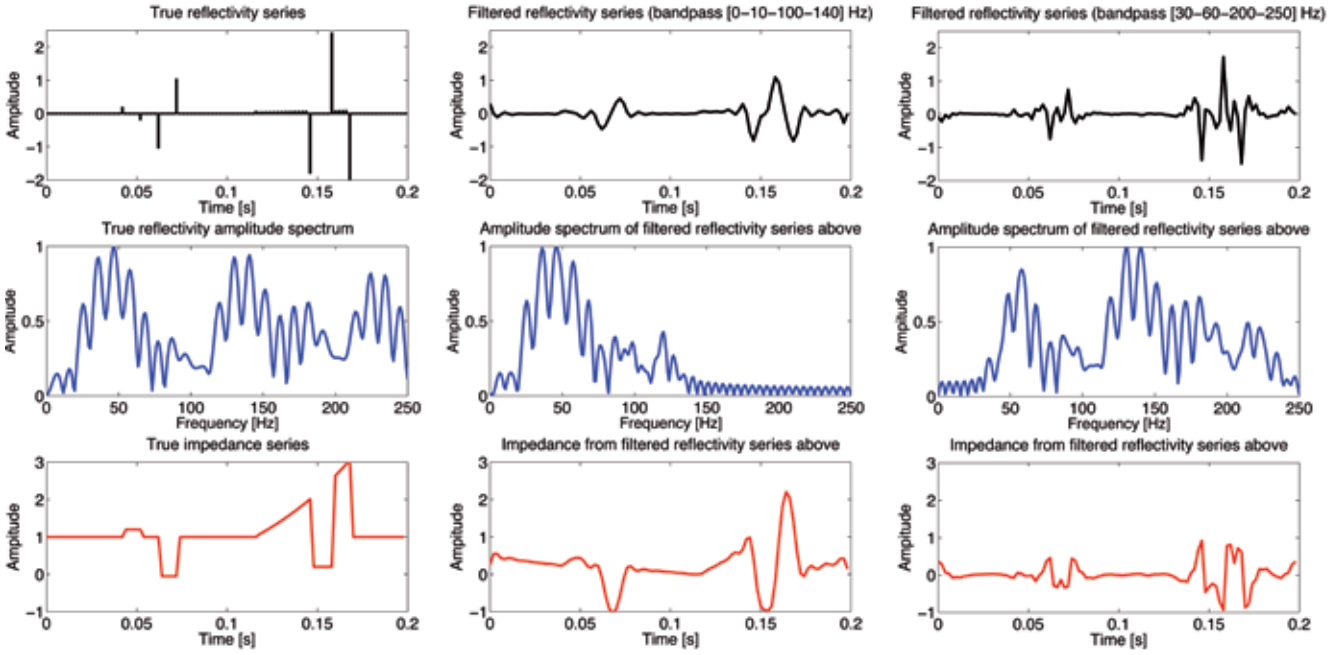

Figure 1 *Synthetic illustration of the impact of reducing bandwidth. (Top row) Reflectivity series, (middle row) amplitude spectra of reflectivity series, and (bottom row) impedance series. (Left column) True reflectivity series, true amplitude spectrum and true impedance series. Note the prominent ramp and step in the impedance series. (Middle column) Filtered reflectivity series, corresponding amplitude spectrum, and impedance series using a 0–10–100–140 Hz bandpass filter. The amplitude spectrum represents that from a 3D seismic survey. After filtering the impedance profile becomes relative and the character is altered. The low amplitude reflection events in the reflectivity series are obscured by the sidelobes that are introduced. (Right column) Filtered reflectivity series, corresponding amplitude spectrum and impedance series using a 30–60–200–250 Hz bandpass filter. The amplitude spectrum represents that from a 'high-resolution' 2D site survey. Removing more low frequency alters the character of the impedance significantly and the ramp is no longer identifiable. The reflectivity series is difficult to interpret due to the introduction of sidelobes, which may be incorrectly perceived as increased resolution.*

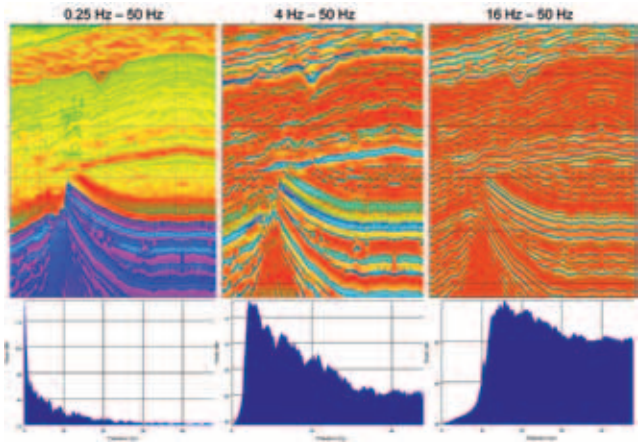

Figure 2 *Bandwidth comparison using synthetic velocity model. The corresponding respective amplitude spectrum is shown below each section. (Left) True synthetic model with high detail spanning approximately eight octaves (0.25 Hz to 50 Hz) bandwidth. (Middle) True synthetic model after high pass filtering to an approximate four octave (4 Hz to 50 Hz) bandwidth. (Right) True synthetic model after high pass filtering to an approximate two octave (16 Hz to 50 Hz) bandwidth. Note the reduction in detail and increase in misleading sidelobe energy that occurs as the bandwidth reduces.*

In the case of the reflectivity series representing a 2D site survey these sidelobes may be incorrectly perceived as increased resolution.

Figure 2 shows a similar bandwidth comparison test to Figure 1, but is performed on a synthetic velocity model generated for evaluating acquisition geometries and velocity inversion technologies (Jones et al., 2012). The true synthetic image has a broad bandwidth of approximately eight octaves (0.25 Hz – 50 Hz). High pass filtering to approximately four octaves (4 Hz – 50 Hz) changes the character of the image considerably; velocity ramps are altered and a halo parallels stepped events. Successive high-pass filtering to approximately two octaves (16 Hz – 50 Hz), which is typical of narrow bandwidth seismic data, further changes the character of events and introduces spurious sidelobes, which could be misinterpreted as increased vertical resolution.

If high-resolution interpretation of geohazards using multiple attributes is desired, maintaining bandwidth in the seismic processing is required. In the next section we review an approach to maintain bandwidth during processing.

Processing to maintain bandwidth

We evaluated current 3D seismic processing flows and identified key areas to focus on for geohazard-specific reprocessing of seismic data. The follow items were considered pertinent:

Source to receiver offset wavelet distortion

Stacking data from different source to receiver offsets to increase the signal to noise ratio (S/N) in the stacked section reduces bandwidth. A decrease in bandwidth occurs due to source to receiver offset dependent stretch of the bandwidth limited wavelet with reflection angle during migration (Tygel et al., 1994 and Levin, 1998), as well as stretch from normal moveout correction (NMO) (Figure 3).

The correction required to flatten a reflection event is related to source to receiver offset and velocity through the hyperbolic model of reflection moveout via the NMO equation. This flattening process necessarily stretches some portions of data more than others, and is most severe for shallow reflection events. However, depending on the S/N a tight full-fold NMO stretch mute (e.g., 5% NMO stretch) can be used to maintain bandwidth (Figure 3).

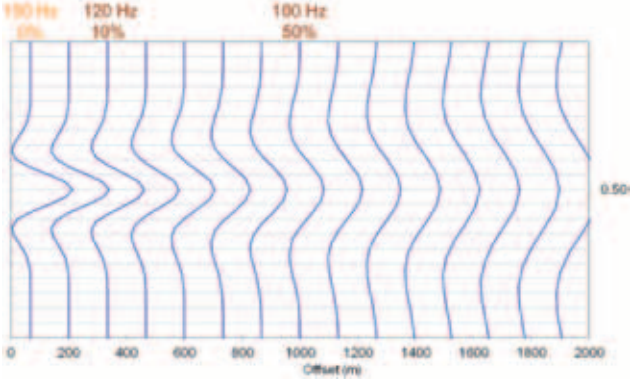

Figure 3 *Illustration showing dominant frequency and NMO stretch as a function of offset for an event at 500 ms and velocity of 1500 m/s. The dominant frequency starts at 150 Hz at 100m offset and 0% NMO stretch. At 300 m offset and 10% NMO stretch the dominant frequency is reduced to 120 Hz. At 1000 m offset and 50% NMO stretch the dominant frequency is reduced to 100 Hz. By stacking a limited offset range the dominant frequency, and bandwidth, can be maintained.*

Plots such as those in Figure 4 can be used to evaluate the likely impact of NMO stretch given the acquisition geometries in varying water depth. These serve as a quick look aid to decide whether reprocessed 3D seismic data just below the water bottom is likely to be usable for geohazard analysis.

Irregular acquisition sampling

Ray-based migrations, such as Kirchhoff schemes, assume regularly sampled data in source and receiver locations, offset and azimuth. These assumptions are addressed by interpolation and regularization prior to migration, to provide a regularly sampled input. Limitations in these schemes cause incomplete cancellation of the migration operator, leading to decreased S/N at higher frequencies and larger geological dips. We observe this decrease in S/N away from the dominant frequency of the seismic data. As we are trying to retain the high frequency content, we attempted to reduce noise at high frequencies by using limited migration apertures and small dip limits (e.g., 3 km migration aperture and 30° dip limit to 1.5 seconds below water bottom).

Oceanographic measurements

In areas of deep water (greater than 300 m) we measure whole water column velocity profiles (collected from veloc-

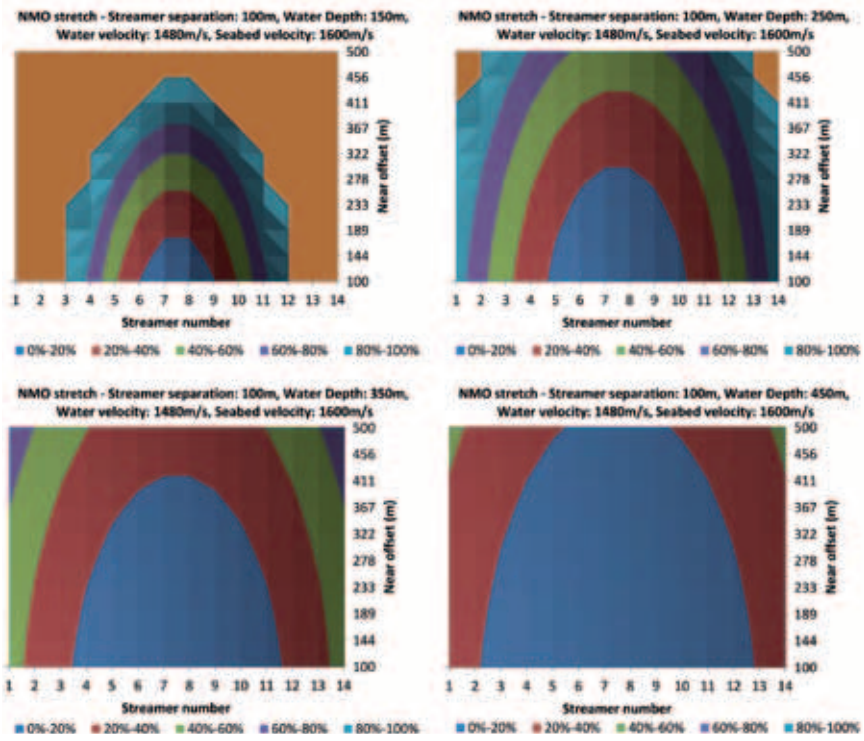

Figure 4 *Evaluation of NMO stretch for a given acquisition geometry. The plots show the NMO stretch percentage (%) across 14 streamers for different near offset distances (m). The streamer separation is fixed at 100 m, the water velocity is fixed at 1480 m/s, and the seabed velocity is fixed at 1600 m/s. The water depth is changed in each plot from 150 m (top left), 250 m (top right), 350 m (bottom left) to 450 m (bottom right). The NMO stretch % is most severe for the shallowest water case.*

ity and depth or salinity, density and depth profilers). These are averaged to form a 3D water velocity field starting from the free surface for use in migration. Shorter period oceanographic changes require the application of water column statics to remove sail-line to sail-line time shifts.

Reprocessing existing 3D seismic data, with special attention paid to the above points, allows bandwidth to be preserved. The next section compares such reprocessed 3D seismic data to 2D site survey data, with a particular focus on horizontal resolution and imaging of dipping events.

2D versus 3D seismic data

Horizontal resolution of seismic data is primarily controlled by the dimensions of the first Fresnel zone; defined as the area of a reflector from which reflected energy arrival times differ by less than half a period from the first arrival, resulting in constructive interference. Migration of seismic data attempts to collapse the Fresnel zone (Lindsey, 1989). One of the major benefits of 3D seismic data is that 3D migration collapses the Fresnel zone in both the inline and crossline directions. In contrast 2D migration collapses the Fresnel zone in the inline (shooting) direction only (Bacon et al., 2007). Consequently, for 2D migrated seismic data the horizontal resolution normal to the direction of shooting equals that of unmigrated data. In other words 2D seismic acquisition and processing is strictly valid only for a 2.5D Earth. Incorrectly assuming zero dip normal to the 2D line leads to coherent artefacts from out-of-plane energy and limits the ability to accurately determine migration velocity. So despite 3D seismic data potentially having lower temporal resolution in the shallow section (compared to 2D site survey seismic data) it has improved spatial resolution.

In Figure 5 we show a comparison between 2D site survey seismic and 3D seismic data that was reprocessed (using the previously described methodology) to preserve bandwidth, referred to as reprocessed 3D seismic data. This figure highlights some of the limitations of using 2D site survey seismic data for geohazard analysis, and, in particular, demonstrates the superior imaging of dipping events provided by the 3D seismic data. Not only is this related to more accurate spatial positioning of energy, but is also a function of increased energy at low frequencies in the broad bandwidth reprocessed 3D seismic data allowing improved fault delineation.

Figure 6 shows the potential for disagreement in lateral positioning of shallow faults on 2D site survey seismic data compared to reprocessed 3D seismic data. The 3D seismic data was extracted along the line geometry of the 2D site survey seismic data to make this comparison possible. This relates to the aforementioned invalid assumption in 2D acquisition and processing of a 2.5D Earth.

Having highlighted the improved horizontal resolution and imaging obtained by reprocessing 3D seismic data, the next two sections show the superior interpretation methods made possible by using 3D seismic data over 2D site survey seismic data.

Global interpretation methods

While the benefits of using 3D seismic data for geohazard analysis have been recognized since at least 1986 (Heggland et al., 1996), the interpretation methodology is usually restricted to analyzing time (or depth) slices, parallel to seabed slices or interpreting selected horizons (Sharp and Samuel, 2004).

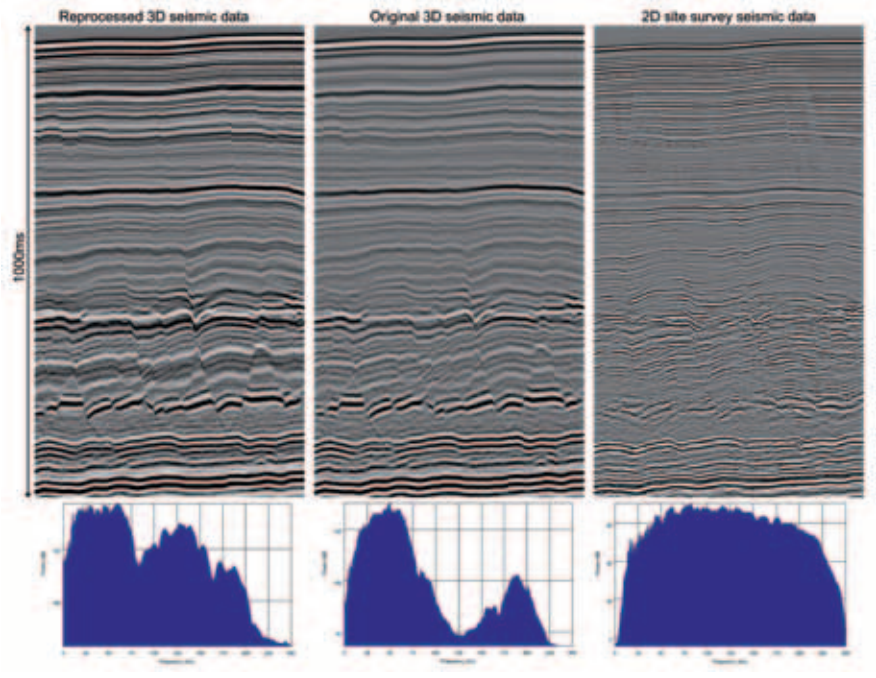

Figure 5 *(Left) Reprocessed 3D seismic data. (Middle) Original 3D seismic data. (Right) 2D site survey seismic data. The corresponding amplitude spectrum is shown below each section. On the reprocessed 3D seismic data note the improved imaging of the deeper faulting that is well within the time range of a site survey investigation.*

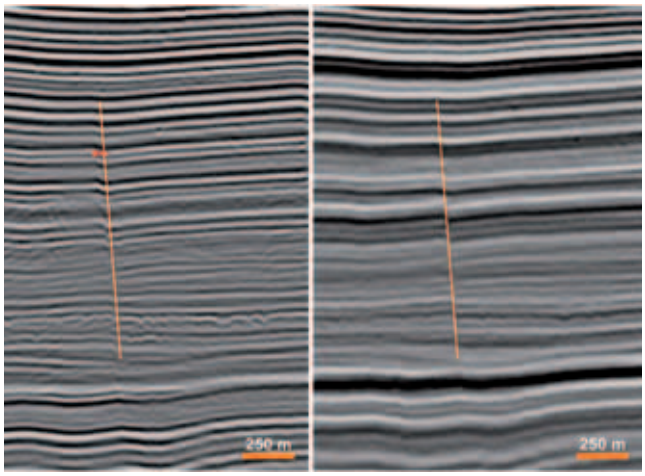

Figure 6 *Comparison of fault imaging between 2D site survey seismic data and reprocessed 3D seismic data. The 3D seismic was extracted along the geometry of the 2D seismic line. (Left) 2D site survey seismic data with fault interpreted on the reprocessed 3D seismic data overlaid. (Right) Reprocessed 3D seismic data with fault interpretation overlaid. The apparent fault positioning differs by 30 m.*

Time slices are suitable for interpreting flat stratigraphy, but there is considerable interpretation ambiguity where stratigraphy dips. If the seabed topography is undulating using parallel to seabed slices can be equally confusing. To avoid this uncertainty it is desirable to perform interpretation following stratigraphy on 'stratal slices'. However, interpreting selected horizons is time-consuming and gives only localized interpretation. Having an interpretation that follows the stratigraphy of the entire shallow section is desirable for geohazard analysis.

A number of techniques for the semi-automatic production of stratal slices from 3D seismic data have been proposed (Zeng et al., 1998; Stark, 2005; Pauget et al., 2009; Fomel, 2010; de Groot et al., 2010; Sherlock and Dorn, 2011). Some of these can be referred to as 'global interpretation methods' since they track every event in the 3D seismic data (Lomask and Guitton, 2007). We have experience of using HorizonCube from dGB Earth Sciences (de Groot et al., 2010) and PaleoScan from Eliis (Pauget et al., 2009). The examples shown in this article were produced using HorizonCube, but the presented methodology may be equally achievable using any global interpretation algorithm. We do not discuss the merits of any particular approach in this article. For further discussion on the benefits and challenges related to stratal slicing of 3D seismic data the interested reader is referred to Zeng (2010). Our main consideration was whether the global interpretation algorithm imposed limitations that restricted the interpretation of the results to one particular software package.

Figure 7 shows a method to produce a global interpretation for the shallow section of 3D seismic data using HorizonCube. Initially a number of horizons are tracked, using either traditional amplitude based autotrackers or a tracker that follows dip (de Groot et al., 2010). These 'anchor horizons' serve to divide the seismic volume into zones with similar seismic character. This enables the parameters for producing intermediate horizons to be tailored to the seismic character within a zone. The HorizonCube algorithm has two ways of generating horizons: model-driven or data-driven. The model-driven approach is based on relationships to bounding horizons and includes 'proportional', 'parallel-

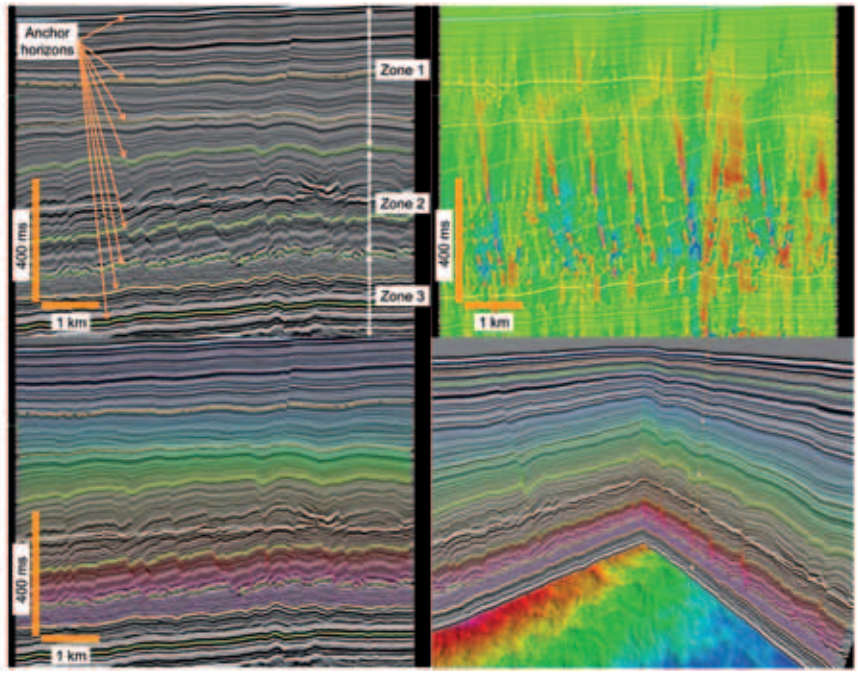

Figure 7 *HorizonCube generation methodology. (Top left) Reprocessed 3D seismic data. White is negative amplitude and this corresponds to an increase in acoustic impedance. Anchor horizons were automatically tracked throughout the reprocessed 3D seismic data. These were located to divide the seismic volume into zones with similar seismic character. This enabled different zones to use different horizon generation techniques, such as model-driven or data-driven. (Top right) Steering cube generated from reprocessed 3D seismic data. This was filtered using a 3D 3x3x3 median filter for use in generating the HorizonCube. The raw steering cube was also used to automatically pick faults. (Bottom left) Generated HorizonCube. Zones 1 and 3 used a data-driven approach; while Zone 2 used a model-driven approach. (Bottom right) Perspective view showing that the generated horizon cube encompasses the whole of reprocessed 3D seismic data. The entire reprocessed 3D seismic data can now be panned through in a pseudo-stratigraphically consistent way.*

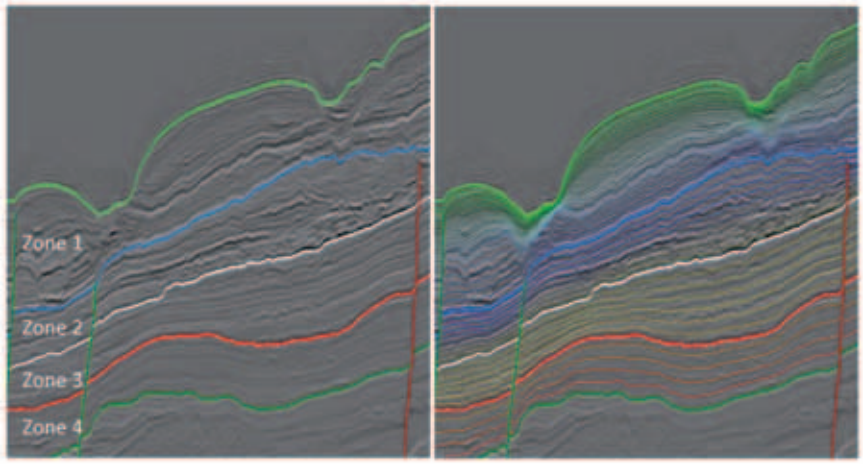

Figure 8 *Another example of HorizonCube generation. (Left) Reprocessed 3D seismic with five anchor horizons and two faults shown. A combination of model-driven (Zone 1) and data-driven (Zones 2, 3 and 4) approaches were used to produce a HorizonCube (right). More geologically complex areas may require further refinement, but the result was acceptable throughout the majority of the 3D seismic volume.*

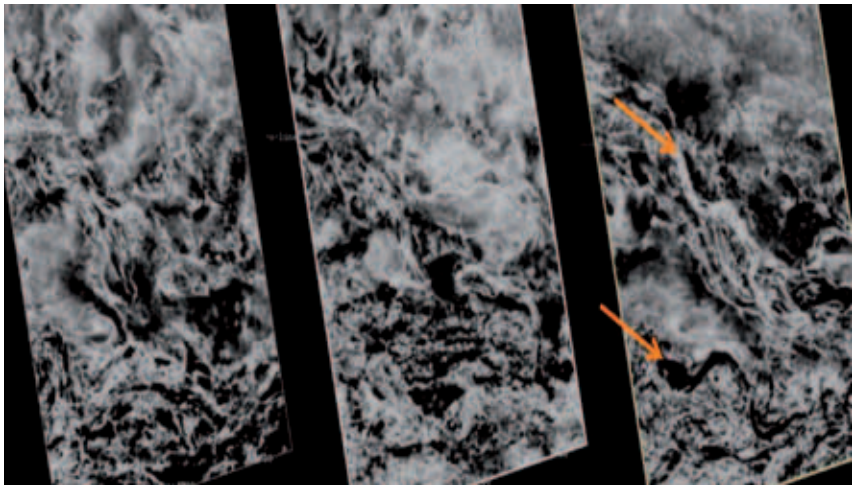

Figure 9 *Comparison of slices in different visualization domains. (Left) Time slice, (middle) seabed flattened slice, and (right) pseudo-stratigraphic slice. These slices are approximately coincident and some common features can be observed on all slices. However the channels are more easily observed on the pseudo-stratigraphic slice as this honours global and local dips.*

to-upper', and 'parallel-to-lower' (Brouwer et al., 2012). The data-driven approach produces horizons by tracking dip and azimuth information. In Figure 7 Zones 1 and 3 used a data-driven approach, while Zone 2 used a model-driven approach. Another example of a HorizonCube generated using reprocessed 3D seismic is shown in Figure 8. Both a model-driven approach (Zone 1) and a data-driven approach (Zones 2, 3 and 4) were used.

Once a satisfactory HorizonCube is constructed it can be used to stratigraphically flatten any attribute of interest. This flattened space is commonly called the Wheeler domain (Stark, 2005). However, we do not claim that we are correctly transforming the seismic data into relative geological time. We are merely applying global interpretation techniques to flatten the seismic according to the local dips such that interpretation ambiguity is reduced. These result in 'pseudo-stratigraphic slices' that can cut through erosional features not conforming to a constant stratigraphy (such as channels), but do highlight potential geohazards.

Typically, we flatten the attributes in the following list for assessment of potential geohazards:

- Seismic amplitude – shallow channels, fluid variation, lithology variation.
- Compressional to shear velocity ratio (Vp/Vs) and acoustic impedance (AI) and/or intercept (I) and gradient (G) – pockmarks, fluid variation, lithology variation, bottom simulating reflectors.
- Similarity – faulting, truncations.
- An anomaly highlighting cube (Edgar and Selvage, 2012).

The flattened volumes can be loaded into any interpretation software along with flattened volumes of two-way time (TWT) or depth for referencing to the unflattened domain.

Reliable prestack information

The 3D pre-stack time migration of the 3D seismic data provides far more reliable amplitude information than 2D pre-stack time migration of 2D seismic, especially in the presence of 3D dip. To benefit from this, pre-stack analysis of the migrated dataset was undertaken to search for geohazards which exhibit changes in amplitude with changes in reflection angle (AVA).

As there were no shallow logged wells located in the area of the seismic data, any pre-stack analysis had to accept the lack of low frequency well-based a-priori information and the inability to estimate deterministic wavelets. This set of conditions would normally favour intercept and gradient analysis. However, this requires equal bandwidth across the gather to avoid artefacts; often achieved by spectral manipulation of the limited angle stacks to match all bandwidths to that of the lowest bandwidth angle stack. As we have tried to maintain the bandwidth of the near offset data, we choose to analyze the pre-stack data using simultaneous pre-stack inversion (Hampson et al., 2005) to avoid having to reduce bandwidth to that of the far offset data.

To estimate the angle-dependent wavelets (5° to 35° in 10° bands) required for simultaneous pre-stack inversion a statistical scheme using kurtosis phase estimation was used (Selvage and Edgar, 2010). The low frequency background models for the inversion were made using a small impedance gradient in time. This results in relative inversion outputs that do not account for compaction effects. Recognizing these limitations of the inversion outputs, their use was constrained to searching for spatial anomalies using crossplots of relative AI against relative Vp/Vs in pseudo-stratigraphically aligned, time-limited windows. This enabled us to search for anomalies within a stratigraphic interval and map their spatial extent.

We have discussed the improved spatial resolution and imaging of reprocessed 3D seismic data over 2D site survey seismic data, and suggested some methods to exploit these benefits during interpretation. The follow section provides some examples of geohazards identified using these methods.

Examples of identified geohazards

The methodologies described above have been successfully applied to 3D seismic data from a variety of geological settings. Examples of potential geohazards identified are shown through Figures 10 to 16.

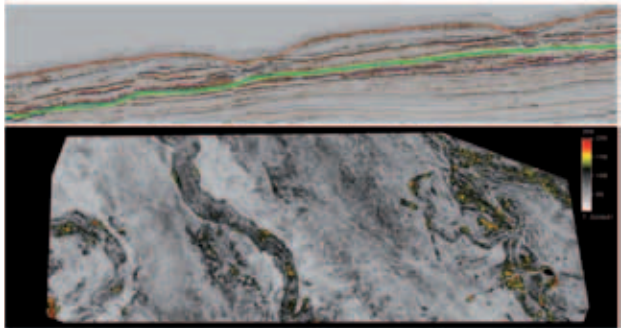

Figure 10 *Example of HorizonCube amplitude extraction. (Top) Seismic section from reprocessed 3D seismic data with a horizon from the HorizonCube overlaid. The seabed is dipping and erosional. (Bottom) Amplitude extraction from reprocessed 3D seismic data along the horizon. Note the spatial continuity of the shallow channels. Such continuity would not be observed on time slices or parallel to seabed slices (Figure 9) and this type of interpretation is not possible on 2D seismic data. Bright amplitudes within the channel fill might be associated with shallow gas hazards.*

A buried infilled channel is shown in Figure 10. The inline section view shows that the seabed has an undulating topography caused by erosional features and that the shallow stratigraphy is dipping. The channel shown in the image below the inline section view is spatially continuous, which gives confidence that the pseudo-stratigraphic slicing is accurate. Such spatial continuity would not be observed on time slices or parallel to seabed slices (Figure 9). Bright amplitudes within the channel fill might be associated with gas and would be flagged as potential geohazards. Further assessment of these bright amplitudes could be based on whether they have anomalous AVA or relative AI and relative Vp/Vs responses.

Seafloor and near-surface faults can be a significant geohazard in many of the deepwater basins that are being explored and developed today (Younes et al., 2005). It was noted that the dip attribute derived from the 3D seismic data was sensitive to faulting (Figure 7). This observation led to the development of an attribute that automatically extracts faults from the seismic dip, which we refer to as a 'fault cube' (Figure 11).

The 2D interpretation of faults is difficult when they are parallel to the 2D line. Faults are easier to recognize on the 3D seismic data thanks to the extra dimension. While it is possible to see curved faults by panning through parallel 2D planes of 3D seismic, they are extremely difficult to interpret in 3D without a methodology that interrogates the data in multiple azimuths. Using 3D volume attributes to generate our fault cube allowed this process to be automated and improves the interpretation (Figures 11 and 12).

Using this fault cube with the pseudo-stratigraphic slices proved to be useful in gaining a more holistic understanding of the seabed topology. Figure 13 demonstrates the strong correlation between the long, linear faults trending north-east to south-west and the seabed long wavelength features. This knowledge may be useful for predicting future shallow fault activation.

King and MacLean (1970) recognized and described pockmarks for the first time as cone-shaped depressions on the seabed. The accepted hypothesis is that pockmarks are formed as a result of gas escaping through the sediments to the seabed, either by seepage (Josenhans et al., 1978) or eruption (Hovland, 1987).

Remnant pockmarks are readily identifiable on pseudo-stratigraphic slices (Figure 14), and with the reprocessed 3D seismic data delineating the spatial extent of individual pockmarks is possible. Having a suite of pseudo-stratigraphic slices also simplifies the investigation of the spatial distribution of multiple pockmarks, the time of pockmark formation, and post formation activity. In addition, while pseudo-stratigraphically panning through flattened attribute volumes of relative Vp/Vs and relative AI, it was noted that pockmarks were anomalous for their stratigraphic level. Therefore, by crossplotting relative Vp/Vs against relative

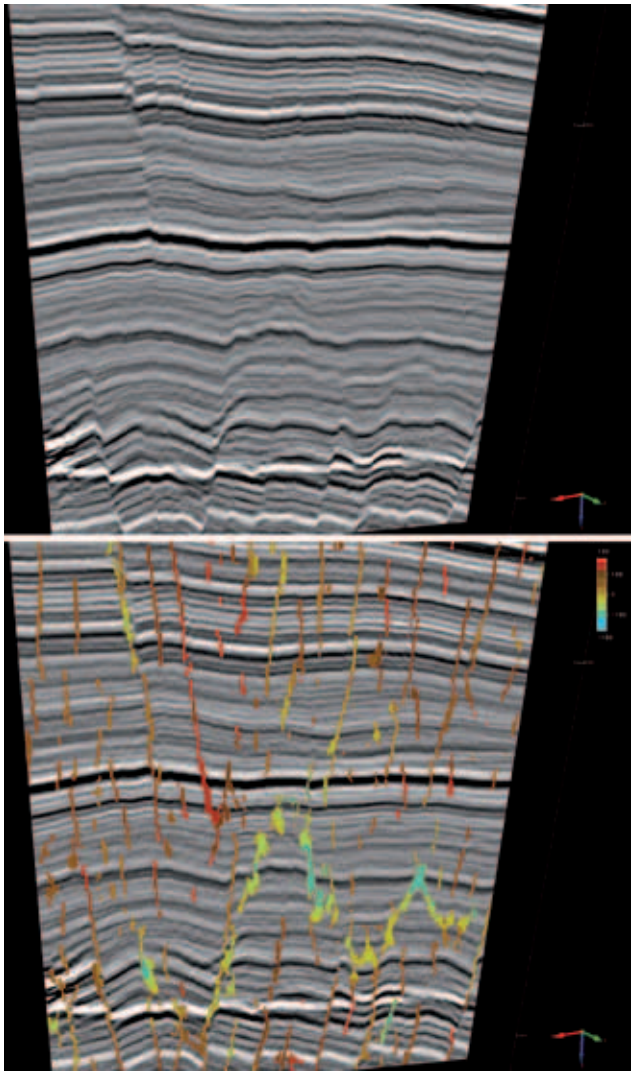

Figure 11 *Example seismic section showing the fault cube result. (Top) Reprocessed 3D seismic section. (Bottom) Overlay of the fault cube on the seismic section. The faults were extracted from the seismic dip data (Figure 7) using a custom attribute set.*

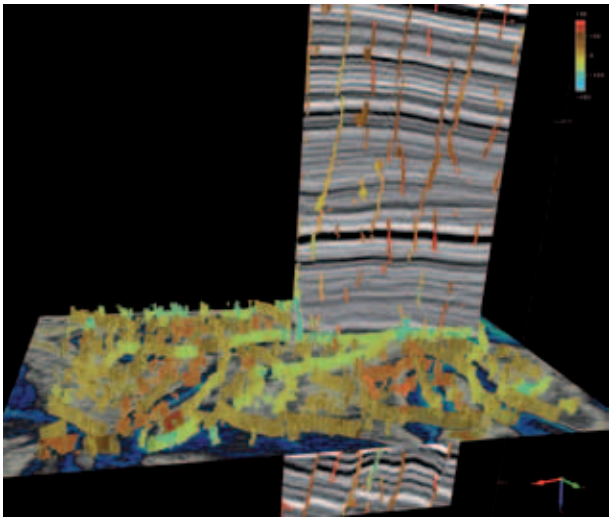

Figure 12 *3D perspective view of the fault cube. The seismic section has faults from the fault cube overlaid. The faults are coloured by azimuth and it can be seen that they are spatially continuous. Interpreting such a complex faulting pattern would be extremely difficult if only 2D data were used, as well as time-consuming and less precise without automating the interpretation method.*

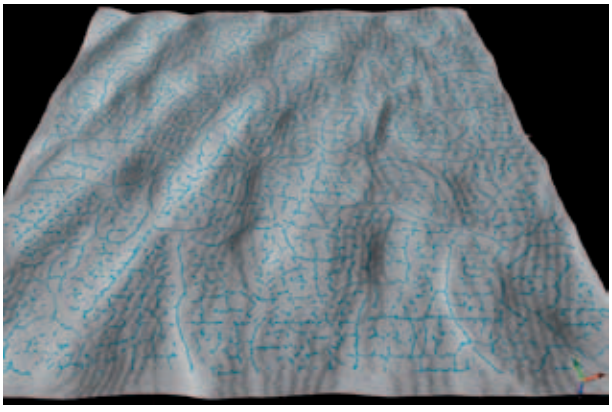

Figure 13 *Example of correlation between the laterally extensive faults and the seabed long wavelength features. The seabed horizon was shifted down by 150 ms and intersections with the fault cube (Figures 11 and 12) are drawn in blue on the seabed horizon.*

AI it would be possible to volume render pockmarks and view their spatial stratigraphic distribution in 3D. This may aid the assessment of pockmark correlation with faulting and, from a geohazard perspective, may aid the assessment of pockmark reactivation (Dimitrov and Dontcheva, 1994).

Bottom simulating reflectors (BSR) can be considered as potential geohazards, for they may be indicative of gas hydrates (Digby, 2005). A possible BSR is observed in the reprocessed 3D seismic data (Figure 15), but is interpreted as the change from opal-A to opal-CT. The reflection event has the same polarity as the seabed and the opal-A to opal-CT transition zone is well documented in this region (Berndt, 2007 and Cartwright, 2007). Since these reflection events cross-cut stratigraphy they are difficult to horizon track and not easy to interpret on pseudo-stratigraphic slices. However, using relative Vp/Vs and relative AI derived from pre-stack seismic data it is possible to volume render the event (Figure 15).

To better evaluate the risks from seafloor instability the survey area needs to be large enough to capture these features, which can be difficult just using 2D surveys. A historic slope failure observed on a pseudo-stratigraphic slice is shown in Figure 16.

Discussion

The examples of potential geohazards in this article demonstrate the level of assessment that is possible using reprocessed 3D seismic data. Such an understanding is unlikely to be achieved from using 2D seismic data alone. For example, mapping or identifying the shallow channels in Figure 10

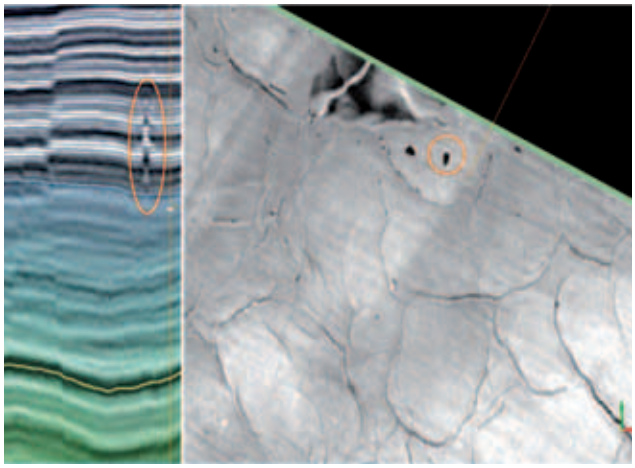

Figure 14 *Example of remnant pockmark identified on a pseudo-stratigraphic slice. The remnant pockmark is highlighted with an orange ellipse. (Left) Seismic section showing HorizonCube horizons. (Right) Amplitude extraction from reprocessed 3D seismic data on a horizon. The horizon cross-cuts the remnant pockmarks, which enables them to be easily delineated on the pseudo-stratigraphic slice. Delineating the extent of these features on 2D seismic data would not be as simple.*

may not be possible from a small 2D site survey seismic dataset. Interpreting the faults in Figures 11 and 12 on 2D seismic data is extremely challenging, time-consuming, and ambiguous. Pre-stack inversion to relative Vp/Vs and relative AI and intercept-gradient analysis from 2D seismic data is unreliable due to amplitude errors caused by the incorrect assumption of zero dip perpendicular to the direction of the 2D line. However, this article can only document in detail a limited subset of the numerous techniques available for interpreting 3D seismic data for geohazard analysis. Other possible methods are briefly discussed below.

Spectral decomposition offers potential to enhance geohazard analysis as is it sensitive to wavelet, reflectivity, tuning and attenuation changes. If the long period wavelet changes could be stabilized then we would be left with changes due to the reflectivity, tuning, and local attenuation. The effects of reflectivity and tuning may then be analyzed in 3D using a pseudo-stratal slice volume to look for tuned reflectors and anomalous changes in reflectivity. Local attenuation is a short temporal effect caused by fluid and/or lithology changes. If this appears as a rapid change in peak frequency then it may be identified on pseudo-stratal slices.

Pore pressure prediction in 3D from seismic velocities presents many challenges. The seismic velocities resulting from travel time tomography or residual NMO analysis is of a much lower vertical resolution than those derived from well logging. Calibrating across such scale differences is difficult and carries a large uncertainty into any pore pressure volume derived from these sources. This is in addition to the uncertainty in seismic stacking velocities, which is commonly compounded further by the assumptions of flat interfaces for the subsequent derivation of both RMS from stacking velocities, and interval from RMS velocities using Dix's Equation. These issues, along with the numerous methods of estimating pore pressure from seismic interval velocities warrant significant further development beyond the scope of this article.

Full waveform inversion (FWI) of marine streamer acquisition shot records offers another potential improvement for geohazard detection. This is in spite of the limited azimuth provided by towed streamer acquisition (Warner et al., 2008). For FWI solutions using refracted seismic wavefields the limited range of source to receiver offsets in streamer data constrains the velocity updates to the shallow subsurface below the water bottom, which is well suited for

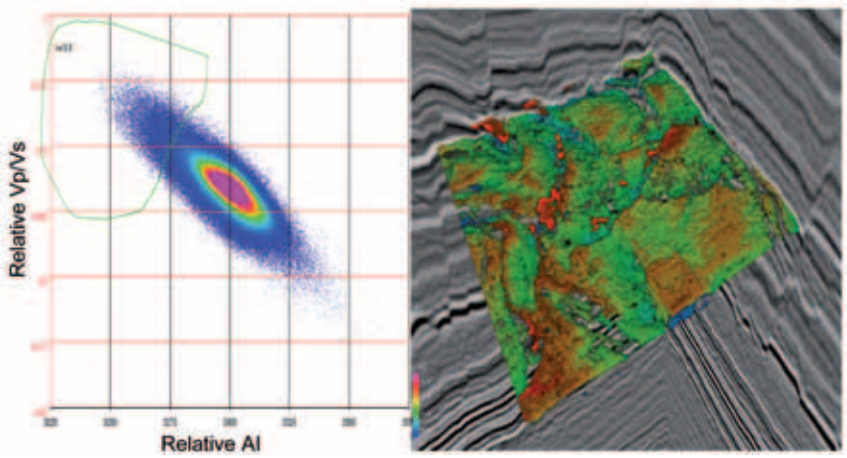

Figure 15 *– Volume rendering of the opal-A to opal-CT transition. (Left) Cross-plot of relative Vp/Vs against relative acoustic impedance (AI). Data within the green polygon was volume rendered. (Right) The opal-A to opal-CT transition is well discriminated using the green polygon cut-off based on relative Vp/Vs against relative AI. The volume rendering is coloured by two-way time (TWT).*

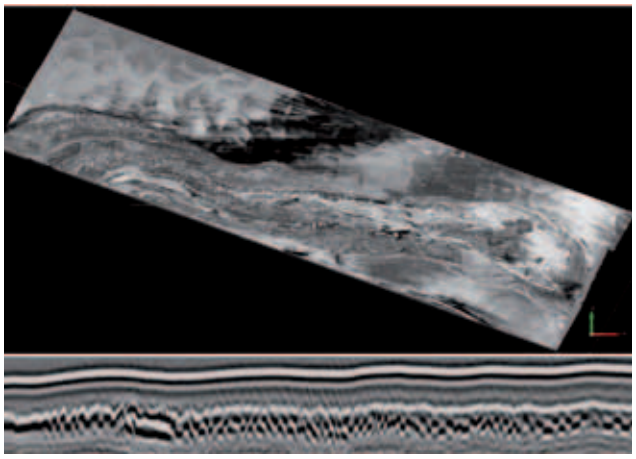

Figure 16 *Example of a historic slope failure on a pseudo-stratigraphic slice. (Top) Amplitude extraction on pseudo-stratigraphic slice through the slump feature. (Bottom) Seismic section showing the slump feature.*

geohazard analysis. Initial results from a test swath have shown correlations between the features in the 3D seismic data and the velocity output from FWI that may provide additional information for geohazard analysis (Figure 17). In this example there appears to be a correlation between faults and slower velocities perpendicular to the sail lines, despite the sail-line parallel artefacts in the velocity output.

The detrimental effect on seismic data bandwidth caused by wavelet stretch (from both the imaging condition varying with receiver incidence angle and NMO stretch) suggests that short source to receiver distance, short channel separation sampling, and shallow cable/source depth are required to get the highest signal to noise ratio at the highest frequency. This is difficult to achieve with industry standard 3D seismic data acquisition. This suggests that a 3D site survey acquisition methodology is required (Sack and Haugland, 2012), which could then be processed together with the existing 3D seismic data to gain all of the 3D benefits demonstrated in this article.

Conclusion

An approach to perform robust and timely identification of geohazards by utilizing existing 3D seismic data has been presented. A short offset reprocessing sequence was used to increase bandwidth over the conventional 3D seismic. A methodology to extract faults from seismic dip data has been created and was used to show the value of 3D data in extracting faults. A global interpretation algorithm was used to produce flattened attribute volumes that are pseudo-stratigraphically consistent and less prone to ambiguity compared to time (or depth) slices, or parallel to seabed slices. Such volumes have been used successfully to assess geohazards in Norway and Tanzania. Performing such an assessment would not be possible if only 2D seismic data was available.

We hope that this article demonstrates the additional information available in 3D seismic data for geohazard analysis and presents automation using global interpretation algorithms to reduce the time needed to locate potential seismic geohazards in ever increasing volumes of seismic data. This enables geohazard specialists to focus on assessing the risk of potential seismic geohazards.

Acknowledgements

The authors thank BG Group for permission to publish this article; Cinzia Scotellaro (BG Group) for her work analyzing the pre-stack data used in this article; BG Norge

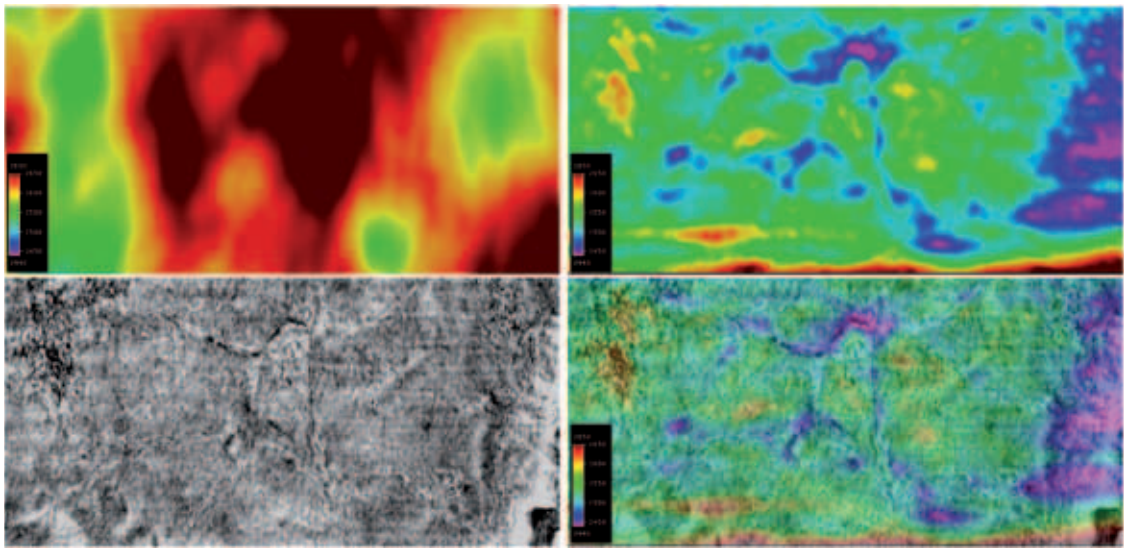

Figure 17 *Full waveform inversion example, (top left) time slice through starting velocity model, (top right) time slice through final velocity model output from FWI, (bottom left) time slice through seismic volume after pre-stack time migration, (bottom right) overlay of velocity model from FWI on the seismic time slice. Correlations between the features in the 3D seismic and the velocity model output from FWI are observed and may provide additional information for geohazard analysis. All time slices are at 300 ms below water bottom. The velocity model colour scales are all the same range.*

and partners in License PL522; BG Norge and partners in Licence PL534; BG Tanzania and partners in Block 1, Block 3, and Block 4; Sophie Mock (CGGV) for processing the 3D seismic for BG Norge and Miles Evans (CGGV) for conducting the FWI trial; James Wright (PGS) for processing the 3D seismic for BG Tanzania; Breandan Murphy (RPS Group), Julie Dickinson (RPS Group), and Karen Ware (RPS Group) for producing the report for BG Norge Licence PL522; Eric Bouanga (dGB Earth Sciences) and Farrukh Qayyum (dGB Earth Sciences) for producing the HorizonCube for BG Tanzania and dGB Earth Sciences for providing support in using OpendTect; Kevin Day (previously of Gardline) and Gardline for performing the geohazard analysis for BG Tanzania using the methodologies outlined in this article.

References

Bacon, M., Simm, R. and Redshaw T. [2007] 3-D Seismic Interpretation. *Cambridge University Press*, 224.

Berndt, C., Bünz, S., Clayton T., Mienert, J. and Saunders, M. [2004] Seismic character of bottom simulating reflectors: examples from the mid-Norwegian margin. *Marine and Petroleum Geology*, **21**(6), 723–733.

Brouwer, F., Huck, A., Hemstra, N. and Braga, I. [2012] Extracting full-resolution models from seismic data to minimize systematic errors in inversion: Method and examples. *The Leading Edge*, **31**(5), 546–554.

Cartwright, J. [2007] The impact of 3D seismic data on the understanding of compaction, fluid flow and diagenesis in sedimentary basin. *Journal of the Geological Society*, **164**(5), 881–893.

Digby, A.J. [2005] Assessment and Quantification of the Hydrate Geohazard. *Offshore Technology Conference*, Houston.

Dimitrov, L. and Dontcheva, V. [1994] Seabed pockmarks in the southern Bulgarian Black Sea zone. *Bull. Geol. Soc. Denmark*, **41**(1), 24–33.

Edgar, J.A. and Selvage, J.I. [2012] Automatic Identification of Seismic Anomalies. *74th EAGE Conference & Exhibition*, Extended Abstract.

Fomel, S. [2010] Predictive painting of 3-D seismic volumes. *Geophysics*, **75**(4), A25–A30.

de Groot, P., Huck, A., de Bruin, G., Hemstra, N. and Bedford, J. [2010] The horizon cube: A step change in seismic interpretation! *The Leading Edge*, **29**(9), 1048–1055.

Hampson, D., Russell, B. and Bankhead, B. [2005] Simultaneous inversion of pre-stack seismic data. *75th SEG Annual International Meeting*, Expanded Abstract.

Heggland, R., Nygaard, E. and Gallagher, J.W. [1996] Techniques and experiences using exploration 3D seismic data to map drilling hazards. *Offshore Technology Conference*, Houston.

Hovland, M. [1989] The formation of pockmarks and their potential influence on offshore construction. *Quarterly Journal of Engineering Geology and Hydrogeology*, **22**, 131–138.

Josenhans, H.W., King, L.H. and Fader, G.B. [1978] A side-scan sonar mosaic of pockmarks on the Scotian Shelf. *Canadian Journal of Earth Sciences*, **15**, 831–840.

Jones, C.E., Edgar, J.A., Selvage, J.I. and Crook, H. [2012] Building Complex Synthetic Models to Evaluate Acquisition Geometries and Velocity Inversion Technologies. *74th EAGE Conference & Exhibition*, Extended Abstract.

King, L. H. and MacLean, B. [1970] Pockmarks on the Scotian Shelf. *Geol. Soc. Am. Bull.* **81**, 3141–3148.

Lindsey, J.P. [1989] The Fresnel zone and its interpretive significance. *The Leading Edge*, **10**, 33–39.

Levin, S.A. [1998] Resolution in seismic imaging: Is it all a matter of perspective? *Geophysics*, **63**(2), 743–749.

Lomask, J. and Guitton, A. [2007] Volumetric flattening: an interpretation tool. *The Leading Edge*, **26**(7), 888–897.

OGP International Associate of Oil & Gas Producers [2011] *Guidelines for the conduct of offshore drilling hazard site surveys*. Available at: <http://www.ogp.org.uk/publications/guidelines-for-the-conduct-of-offshore-drilling-hazard-site-surveys/> (Accessed 23 June 2012).

Pauget, F., Lacaze, S. and Valding, T. [2009] A Global Approach to Seismic Interpretation Based on Cost Function Minimization. *79th SEG Annual International Meeting*, Expanded Abstract, **28**(1), 2592–2596.

Sack, P. and Haugland, T.A. [2012] Development of a Multistreamer 3D High Resolution System. *74th EAGE Conference & Exhibition*, Extended Abstract.

Selvage, J.I. and Edgar, J.A. [2010] Estimating Non-stationary Wavelet Phase and Phase Error. *72nd EAGE Conference & Exhibition*, Extended Abstract.

Sharp, A. and Samuel, A. [2004] An example study using conventional 3D seismic data to delineate shallow gas drilling hazards from the West Delta Deep Marine Concession, offshore Nile Delta, Egypt. *Petroleum Geoscience*, **10**(2), 121–129.

Sheriff, R.E. [1991] *Encyclopedic Dictionary of Exploration Geophysics*. Society of Exploration Geophysicists, 3rd Edition, 384.

Sherlock, K.L.S and Dorn, G.A.D. [2011] Stratal Domain Transformation - A Workflow. *73rd EAGE Conference & Exhibition*, Extended Abstract.

Stark, T.J. [2005] Generation of a 3D seismic "wheeler diagram" from a high resolution age volume. *75th SEG Annual International Meeting*, Expanded Abstract, **24**(1), 782–785.

Tygel, M., Schleicher, J. and Hubral, P. [1994] Pulse distortion in depth migration, *Geophysics*, **59**(10), 1561-1569.

Warner, M., Stekl, I. and Umpleby, A. [2008] Efficient and Effective 3D Wavefield Tomography. *70th EAGE Conference & Exhibition*, Extended Abstract.

Younes, A.I., Gibson, J.L. and Shipp, R.C. [2005] Geohazard Assessment of the Deepwater Princess Field in the Northeastern Gulf of Mexico: Example of Evaluating Complex Faulting in a Subsea Development. *Offshore Technology Conference*, Houston.

Zeng, H., Henry S.C. and Riola, J. P. [1998] Stratal slicing, part II: Real 3-D seismic data. *Geophysics*, **63**, 514–522.

Zeng, H. [2010] Stratal slicing: benefits and challenges. *The Leading Edge*, 29(9), 1040–1047.